Classification: Major: Physical Sciences, Minor: Engineering

Scalable ultrasound directed self-assembly of user-specified patterns of nanoparticles dispersed in a fluid medium

J. Greenhall[1], F. Guevara Vasquez[2], B. Raeymaekers[1*]

[1]*Department of Mechanical Engineering, University of Utah, Salt Lake City, UT, USA*

[2]*Department of Mathematics, University of Utah, Salt Lake City, UT, USA*

Abstract

We employ an ultrasound wave field generated by one or more ultrasound transducers to organize large quantities of nanoparticles dispersed in a fluid medium into two-dimensional user-specified patterns. To accomplish this, we theoretically derive a direct method of calculating the ultrasound transducer parameters required to assemble a user-specified pattern of nanoparticles. The computation relates the ultrasound wave field and the force acting on the nanoparticles to the ultrasound transducer parameters by solving a constrained optimization problem. We experimentally demonstrate this method for carbon nanoparticles in a water reservoir and observe good agreement between experiment and theory. This method works for any simply-closed fluid reservoir geometry and any arrangement of ultrasound transducers, and it enables using ultrasound directed self-assembly as a scalable fabrication technique that may facilitate a myriad of engineering applications, including fabricating engineered materials with patterns of nanoscale inclusions.

Keywords: ultrasound, directed self-assembly, engineered materials

*bart.raeymaekers@utah.edu

Significance statement (120 words max)

Ultrasound directed self-assembly enables organizing large quantities of nanoparticles into patterns using an ultrasound wave field generated by one or more ultrasound transducers. While critical to using this technique, no method exists to tune the parameters of ultrasound transducers to obtain a user-specified pattern of nanoparticles. We demonstrate a method of calculating the ultrasound transducer parameters required to assemble a user-specified pattern of nanoparticles in a fluid medium. In contrast with existing methods, which are limited to specific ultrasound transducer arrangements and pattern geometries, our method provides a universal solution. This work has implications for employing ultrasound directed self-assembly as a fabrication technique for engineered materials with patterns of nanoscale inclusions, including dielectric metamaterials and nanocomposite materials.

Introduction

Directed self-assembly (DSA) is defined as the process by which nanoparticles or other discrete components organize as a result of interactions between the components themselves and/or with their environment[1]. DSA is typically divided into three categories: templated, template-free, and external field-directed techniques. Templated DSA involves surface-modified substrates that selectively prompt nanoparticle deposition into user-specified patterns[2]. Macroscale templates are obtained using block-copolymer substrates with complex chemical functionalization for compatibility with the nanoparticles[3]. Template-free DSA methods use capping molecules that selectively interact with each other and with the nanoparticles to create organized patterns of nanoparticles[1]. The pattern geometries that can be obtained are limited by the properties of the capping molecules and the nanoparticles[4]. External field-directed techniques including electric[5], magnetic[6], or ultrasound fields[7] are also used to assemble patterns of nanoparticles suspended in a fluid medium. The external field is generated by a set of transducers and acts as a tunable mask, enabling the pattern of nanoparticles to be modified by adjusting the arrangement and parameters of the transducer(s). Electric and magnetic fields require using conductive and ferromagnetic nanoparticles, respectively, and demand an ultra-high field strength to organize the nanoparticles into user-specified patterns[8,9], thus limiting scalability. Alternatively, ultrasound DSA relies on the acoustic radiation force associated with an ultrasound (pressure) field to organize nanoparticles into user-specified patterns. This technique works independent of material properties[7], and weak attenuation of ultrasound waves in most low-viscosity fluids reduces the need for ultra-high field strengths, thus enabling scalability[7,10].

Ultrasound DSA could enable fabricating complex multi-dimensional patterns of nanoparticles for use in a wide range of engineering applications including biology[11], biomedical devices[12], process control[13], and bottom-up manufacturing of engineered nanostructured materials with exotic properties[14-17]. However, using ultrasound DSA as a fabrication technique requires relating the ultrasound transducer arrangement and parameters that generate the ultrasound wave field to the resulting patterns of nanoparticles that are assembled. This translates into two problems: (1) the “forward problem” entails

calculating the pattern of nanoparticles resulting from user-specified ultrasound transducer parameters, and (2) the "inverse problem" involves calculating the ultrasound transducer parameters required to assemble a user-specified pattern of nanoparticles.

The forward problem is solved by computing the acoustic radiation force associated with the ultrasound wave field generated by the ultrasound transducers. The resulting pattern of nanoparticles is then found as the stable fixed points $\mathbf{x}_f$ of the acoustic radiation force, defined as the location(s) where the force is zero and points toward $\mathbf{x}_f$ in the surrounding region[18]. The inverse problem is solved either directly or indirectly. Indirect methods rely on solving the forward problem for a range of ultrasound transducer parameters to create a "map" of nanoparticles patterns that can be assembled as a function of those parameters[19-21]. Direct methods on the other hand have only been derived for a limited number of specific cases, including dot patterns in circular reservoirs lined with ultrasound transducers[22,23]. However, these existing methods fail to provide a universal solution to the inverse problem. Thus, the objective of this work is to demonstrate and experimentally validate a direct solution methodology to the inverse problem for a user-specified pattern within a two-dimensional reservoir with an arbitrary simply-closed geometry and ultrasound transducer arrangement. This is critical to enabling ultrasound DSA as a fabrication technique.

We relate the user-specified patterns of nanoparticles to the ultrasound transducer parameters in two steps. First we calculate the ultrasound wave field in an arbitrary shaped reservoir lined with ultrasound transducers around its perimeter as a function of the transducer parameters using the boundary element method based on Green's third identity[24], which relates the wave field within a simply-closed domain to the boundary conditions imposed on the perimeter of that domain. Then, we apply Gor'kov's method[18,25] of calculating the acoustic radiation force acting on a spherical particle to determine the pattern of nanoparticles resulting from the ultrasound wave field. Finally, we compute the ultrasound transducer parameters required to assemble a user-specified pattern of nanoparticles by solving a constrained optimization problem using eigendecomposition. We present a theoretical derivation and experimental validation.

Model

Figure 1 shows a two-dimensional arbitrary shaped reservoir filled with a fluid medium of density ρ_m and sound speed c_m, and with N_t ultrasound transducers of acoustic impedance Z_t around the perimeter. The inset of Fig. 1 illustrates the discretization of the domain perimeter S into $N_b \geq N_t$ boundary elements (black dots) and the domain D into N_d domain points (red dots), which may be selected in any arrangement. The j^{th} boundary element, identified by its center point $\mathbf{q}_j$, is $\varepsilon(\mathbf{q}_j)$ wide and is driven by the ultrasound transducer parameter $v(\mathbf{q}_j)$, i.e., the complex harmonic velocity (amplitude and phase) of the transducer surface along its normal direction $\mathbf{n}(\mathbf{q}_j)$, which acts as a piston source to create the ultrasound wave field. Additionally, we indicate a test point $\mathbf{x}_l$ in D with respect to the reservoir origin $\mathbf{o}$.

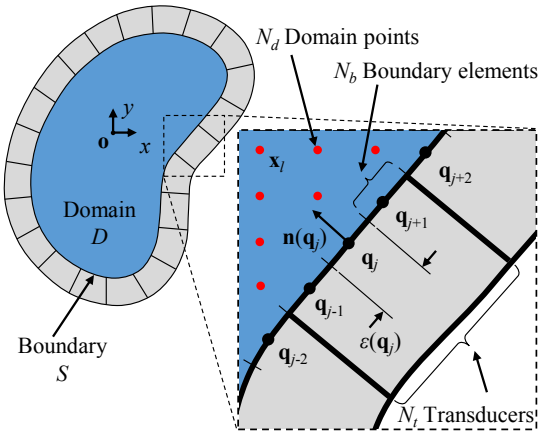

Figure 1: Two-dimensional arbitrary shaped fluid reservoir lined with N_t ultrasound transducers. The inset illustrates the discretization scheme of the boundary element method, dividing the domain perimeter into N_b boundary elements (black dots) and the domain into N_d domain points (red dots). Additionally, the inset shows the width $\varepsilon(\mathbf{q}_j)$ and normal direction $\mathbf{n}(\mathbf{q}_j)$ of the j^{th} boundary element centered at $\mathbf{q}_j$.

We use the boundary element method to calculate the ultrasound wave field with frequency ω_0 in terms of the time-independent, complex scalar velocity potential φ, at each domain point within D. We note that: (1) φ must be a wave and, thus, satisfy the Helmholtz equation ($\nabla^2\varphi + k_0^2\varphi = 0$) in D, where $k_0 = \omega_0/c_m$ is the wave number of the ultrasound wave field in the fluid medium. (2) The impedance boundary condition $\partial\varphi/\partial\mathbf{n} + ik_0\tilde{Z}\varphi = v$ must be satisfied on S, where $\tilde{Z} = \rho_m c_m/Z_t$ is the impedance ratio, accounting

for the absorption and reflection of the ultrasound wave within the fluid medium as it interacts with the ultrasound transducer surface[25]. Arranging all ultrasound transducer parameters v into a vector $\mathbf{v}$, we calculate the ultrasound wave field at all N_d domain points as a single vector[24]

$$\boldsymbol{\varphi} = \mathbf{PWv}\,. \tag{1}$$

The matrix $\mathbf{W}$ maps each boundary element to its corresponding ultrasound transducer, i.e., $w_{jm} = 1$ if the j^{th} boundary element is contained within the m^{th} transducer, otherwise $w_{jm} = 0$. Additionally, each term p_{lj} of the matrix $\mathbf{P}$ corresponds to the ultrasound wave field created at $\mathbf{x}_l$ by a point source located at $\mathbf{q}_j$ on S, including all reflections from the reservoir walls. We calculate all p_{lj} terms in matrix form as

$$\mathbf{P} = \hat{\mathbf{B}} - \hat{\mathbf{A}}\left(\tfrac{1}{2}\mathbf{I} + \mathbf{A}\right)^{-1}\mathbf{B}, \tag{2}$$

for all N_d domain points. $\mathbf{I}$ is the identity matrix and we compute each term a_{lj} and b_{lj} of the matrices $\mathbf{A}$ and $\mathbf{B}$ as

$$a_{lj} = \left[ik_0\bar{Z}G\left(\mathbf{q}_j,\mathbf{x}_l\right) + \frac{\partial G\left(\mathbf{q}_j,\mathbf{x}_l\right)}{\partial \mathbf{n}(\mathbf{q}_j)}\right] \times \varepsilon\left(\mathbf{q}_j\right)\delta\left(\mathbf{q}_j,\mathbf{x}_l\right), \text{ and} \tag{3}$$

$$b_{ij} = G\left(\mathbf{q}_j,\mathbf{x}_l\right)\varepsilon\left(\mathbf{q}_j\right)\delta\left(\mathbf{q}_j,\mathbf{x}_l\right). \tag{4}$$

Here, $i = (-1)^{1/2}$, $\delta(\mathbf{q}_j, \mathbf{x}_l) = 0$ when $\mathbf{q}_j = \mathbf{x}_l$, otherwise it is 1, and $G(\mathbf{q}_j,\mathbf{x}_l)$ is the Green's function, which represents the free-field ultrasound wave emitted from a point-source located at $\mathbf{q}_j$ and measured at location $\mathbf{x}_l$, defined as[24]

$$G\left(\mathbf{q}_j,\mathbf{x}_l\right) = -\frac{i}{4}H_0\left(k_0\left|\mathbf{q}_j - \mathbf{x}_l\right|\right). \tag{5}$$

H_0 is the 0^{th} order Hankel function of the first kind, and $|\mathbf{q}_j - \mathbf{x}_l|$ is the Euclidean distance between points $\mathbf{q}_j$ and $\mathbf{x}_l$. We obtain the matrices $\hat{\mathbf{A}}$ and $\hat{\mathbf{B}}$ in Eq. (2) analogously to $\mathbf{A}$ and $\mathbf{B}$, differing only by the selection of the points $\mathbf{x}_l$, which lay on S for $\mathbf{A}$ and $\mathbf{B}$, and lay in D for $\hat{\mathbf{A}}$ and $\hat{\mathbf{B}}$. Thus, using the boundary element method we relate the ultrasound transducer parameters to the resulting ultrasound wave field.

To relate the ultrasound wave field to the pattern of nanoparticles, we calculate the acoustic radiation force acting on a nanoparticle of density ρ_p and sound speed c_p, dispersed in a fluid medium at location $\mathbf{x}_l$ in D as

$$\mathbf{f}_l = -\nabla U_l, \tag{6}$$

where U_l is the acoustic radiation potential in $\mathbf{x}_l$. For a spherical particle with radius $r_p \ll \lambda_0$, where $\lambda_0 = 2\pi c_f/\omega_0$, we compute U_l as[18,25]

$$U_l = \mathbf{v}^H \mathbf{Q}_l \mathbf{v}, \tag{7}$$

where $\mathbf{v}^H$ is the conjugate transpose of $\mathbf{v}$, and the Hermitian matrix $\mathbf{Q}_l$ is calculated as

$$\mathbf{Q}_l = 2\pi r_p^3 \rho_m \mathbf{W}^H \left\{ \frac{1}{3} k_0^2 \left[1 - \left(\frac{\beta_p}{\beta_m} \right)^2 \right] \left[\mathbf{p}_l \mathbf{p}_l^H \right] - \left[\frac{\rho_p - \rho_m}{2\rho_p + \rho_m} \right] \left[\left(\nabla \mathbf{p}_l \right) \left(\nabla \mathbf{p}_l \right)^H \right] \right\} \mathbf{W} \tag{8}$$

$\mathbf{p}_l^H$ is the l^{th} row of $\mathbf{P}$, and $\beta_m = 1/\rho_m c_m$ and $\beta_p = 1/\rho_p c_p$ are the compressibility of the fluid medium and particle, respectively. From Eq. (7), we calculate the obtained pattern of nanoparticles as the region(s) consisting of points $\mathbf{x}_l$, where U_l is locally minimum. Thus, to achieve assembly of a user-specified pattern of nanoparticles consisting of the set of desired positions X_{des}, each value U_l corresponding to each position $\mathbf{x}_l \in \mathrm{X}_{des}$, must be locally minimum. We relax the requirement of local minimality to obtain an optimization problem with a single objective function. Instead, we aim to minimize the average value of U_l over all points $\mathbf{x}_l \in \mathrm{X}_{des}$, which is written as the quadratic function

$$\bar{U} = \mathbf{v}^H \bar{\mathbf{Q}} \mathbf{v}, \tag{9}$$

where the matrix $\bar{\mathbf{Q}}$ is the average of the matrices $\mathbf{Q}_l$ corresponding to each desired position $\mathbf{x}_l \in \mathrm{X}_{des}$. $\bar{U}$ has no lower bound because the matrix $\bar{\mathbf{Q}}$ is indefinite. Physically, this occurs because particles are assembled at the desired positions more effectively by increasing the harmonic velocity amplitudes of the ultrasound transducer surfaces indefinitely ($|\mathbf{v}| \to \infty$). Practically, the function generator that energizes the ultrasound transducers limits the harmonic velocity amplitudes of the transducer surfaces to finite values

and, thus, we constrain the magnitude $|\mathbf{v}| = \alpha$, where α is a real, scalar value representing the maximum harmonic velocity of the ultrasound transducer surface that can be achieved with a function generator. Hence, we formulate the constrained quadratic optimization problem

$$\min \bar{U}, \text{ subject to } |\mathbf{v}| = \alpha. \tag{10}$$

From Eq. (10), we calculate the ultrasound transducer parameters **v*** required to assemble a user-specified pattern of nanoparticles as the eigenvector corresponding to the smallest eigenvalue of $\bar{\mathbf{Q}}$, where **v*** has length α[26].

Results and discussion

To demonstrate assembly of a complex user-specified pattern of nanoparticles, we define the University of Utah "U" logo within a square 12.75×12.75 mm water-filled reservoir with N_t = 200 transducers ($\omega_0/2\pi$ = 750 kHz) around the perimeter, and compute the ultrasound transducer parameters **v*** required to assemble this pattern using Eq. (10). Figure 2 shows the simulated pattern of nanoparticles resulting from the computed ultrasound transducer parameters **v*** (black) and the corresponding acoustic radiation potential (green), together with the user-specified "U" pattern (red). We qualitatively observe a close match between the user-specified and simulated patterns, except at sharp edges. Extra features not part of the user-specified pattern may exist if the optimization (Eq. (10)) does not yield an exact match with the user-specified pattern for the specified ultrasound transducer arrangement, operating frequency ω_0, and reservoir geometry.

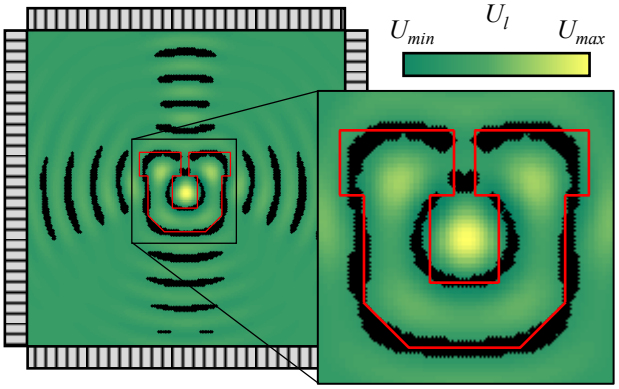

Figure 2: Simulated University of Utah "U" logo pattern of nanoparticles (black), and corresponding acoustic radiation potential (green) obtained by applying the computed ultrasound transducer parameters **v*** required to assemble a user-specified "U" pattern (red) to the ultrasound transducer arrangement.

Fig. 2 illustrates that complex patterns of nanoparticles can be assembled using this method, but large numbers of ultrasound transducers are often required. To experimentally validate our model and method, we limit the number of transducers to N_t = 4 and 8 and focus on dot and line patterns of nanoparticles. Figure 3 shows a schematic of the experimental validation procedure. We define a user-specified pattern in a square reservoir filled with water and 80 nm carbon nanoparticles, lined with PZT transducers (type SM112) with center frequency of $\omega_0/2\pi$ = 1.5 MHz. We compute the ultrasound transducer parameters **v*** to obtain the user-specified pattern using the inverse method by solving Eq. (10). These parameters $\mathbf{v}^* = [v_1, v_2, \ldots, v_{Nt}]^T$ are applied to the N_t transducers using a function generator, and we record the assembled pattern of nanoparticles using a camera, and compare it to the initial user-specified pattern.

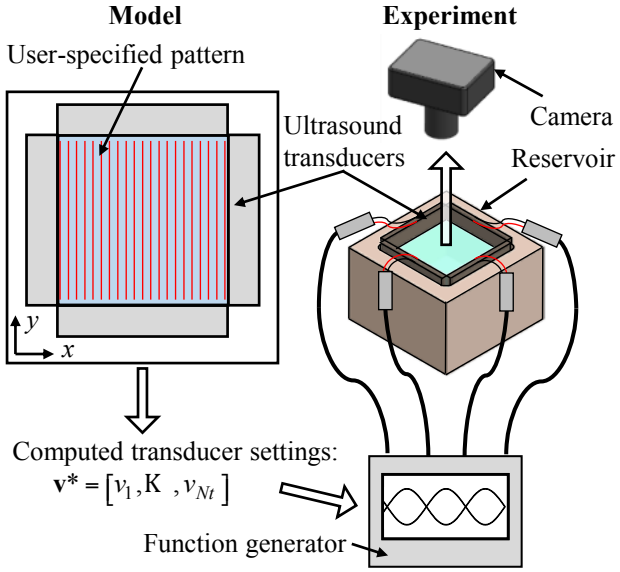

Figure 3: Validation of the method using a square reservoir filled with water and dispersed 80 nm carbon particles. A user-specified pattern is defined in the model and the ultrasound transducer parameters to obtain this pattern are computed using the inverse method. The ultrasound transducer parameters are then applied to the experimental set-up, assembling a pattern of nanoparticles that is compared to the user-specified pattern.

Figure 4 shows two example patterns in a 12.75×12.75 mm square reservoir with N_t = 4. Feasible patterns for this ultrasound transducer arrangement include lines spaced $\lambda_0/2$ apart, parallel to a reservoir

wall (Fig. 4(a)), and dots arranged in a square grid formation spaced $\lambda_0/2$ apart (Fig. 4(b)). Additionally, using a 24.75×24.75 mm square reservoir with $N_t = 8$ enables assembly of more complex patterns, such as a shifted line pattern (Fig. 5(a)), and a mixed line/dot pattern (Fig. 5(b)). In Figs. 4 and 5, we show an image of the experimentally obtained pattern after computing and applying the ultrasound transducer parameters, superimposed with the user-specified pattern in red. The insets show a magnified view, and the tables list the calculated ultrasound transducer parameters **v***, i.e., the amplitude and phase of the harmonic velocity of the ultrasound transducer surface.

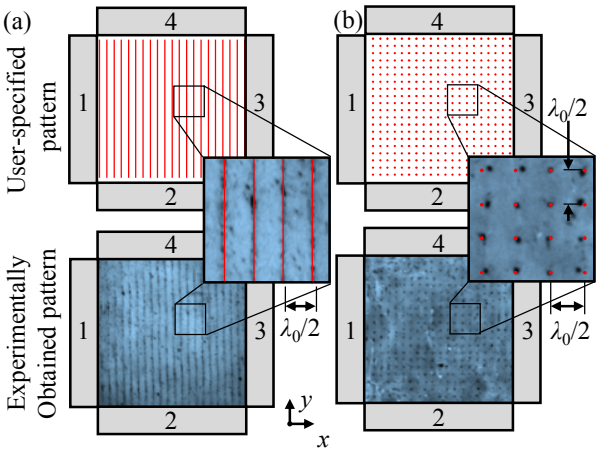

T	Amplitude [m/s]	Phase [deg.]
1	0.70	-141.3
2	0.00	0.0
3	0.71	-143.0
4	0.00	0.0

T	Amplitude [m/s]	Phase [deg.]
1	0.50	180.0
2	0.50	-2.3
3	0.50	177.7
4	0.50	0.0

Figure 4: Experimental results showing the user-specified patterns (red) and experimentally obtained patterns (black) assembled with the ultrasound transducer parameters calculated using Eq. (10) for a (a) line pattern, (b) dot pattern of nanoparticles. The tables list the calculated ultrasound transducer parameters **v*** to assemble the pattern of nanoparticles.

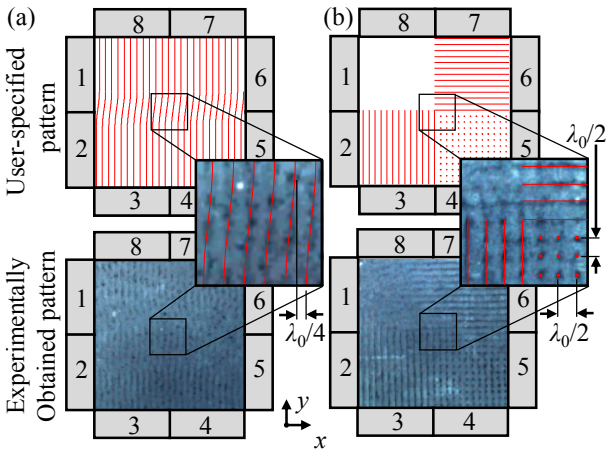

T	Amplitude [m/s]	Phase [deg.]
1	0.00	180.0
2	0.49	32.3
3	0.00	0.0
4	0.51	32.3
5	0.51	32.3
6	0.00	-180.0
7	0.49	32.3
8	0.00	0.0

T	Amplitude [m/s]	Phase [deg.]
1	0.69	0.0
2	0.15	-15.4
3	0.00	0.0
4	0.00	0.0
5	0.69	0.0
6	0.15	-15.4
7	0.00	180.0
8	0.00	180.0

Figure 5: Experimental results showing the user-specified patterns (red) and experimentally obtained patterns (black) assembled with the ultrasound transducer settings calculated using Eq. (10) for a (a) shifted line pattern, (b) mixed line/dot pattern of nanoparticles. The tables list the calculated ultrasound transducer parameters **v*** to assemble the pattern of nanoparticles.

To quantify the accuracy of the experimentally assembled pattern of nanoparticles with respect to the inverse problem solution calculated with the model, we specify line and dot patterns at positions shifted along the x- and y- direction over a distance $\Delta x \in [0, \lambda_0/2)$. We calculate the pattern error E_{pat} as the average distance between the centers of the user-specified and experimentally obtained pattern features (lines or dots), normalized by the nominal pattern spacing $\lambda_0/2$. Figure 6 shows the pattern error as a function of the normalized pattern shift distance $\Delta x/\lambda_0$ for line (triangle marker) and dot (dot marker) patterns, in addition to images of the user-specified patterns superimposed on the experimentally obtained patterns, for line and dot patterns shifted by $\Delta x/\lambda_0 = \{0.000, 0.250, 0.438\}$. We observe that the pattern error E_{pat} is less than 16.0% and 16.5% for line and dot patterns, respectively, indicating good agreement between the user-specified and experimentally assembled patterns of nanoparticles. In practice, these patterns are not identical due to e.g. manufacturing imperfections in the experimental setup that affect the

resulting ultrasound wave field. Additionally, the model neglects viscous, thermal, and electrostatic effects. We also note that it is possible for the experimentally obtained pattern to contain additional pattern features, not part of the user-specified pattern. For instance, it is possible to assemble a user-specified dot pattern with spacing $\lambda_0/2$ by producing a line pattern that passes through the desired dot locations. In these instances, the pattern error is insufficient to account for the additional features, and a more complex scoring algorithm, such as a template matching method used in image processing[27], is desirable.

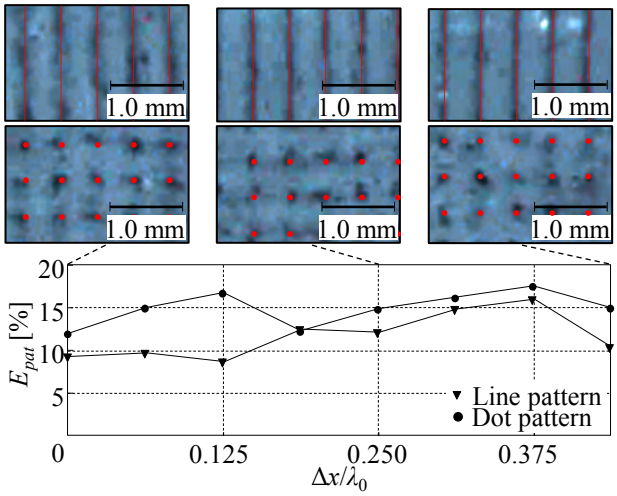

Figure 6: Pattern error E_{pat} for user-specified line and dot patterns shifted with increments of $\Delta x/\lambda_0 = 0.0625$. Insets show images of the user-specified and experimentally obtained line and dot patterns for $\Delta x/\lambda_0 = \{0.000, 0.250, 0.438\}$.

Conclusion

We have derived, for the first time, a direct solution method that relates a user-specified pattern of nanoparticles in a fluid medium contained in an arbitrary shaped reservoir, to the operating parameters of any arrangement of ultrasound transducers, enabling ultrasound directed self-assembly as a fabrication technique. We observe good agreement between theory and experiments. This work contrasts with existing indirect methods, which require calculating complex maps of feasible patterns, and direct methods, which only work for a limited set of reservoir geometries and pattern geometries. In addition, our method accounts for all reflected waves, enabling experimental validation without requiring a complex setup with matching and backing layers to eliminate reflections. Thus, this method provides a

practical approach of creating a user-specified pattern of nanoparticles using an arrangement of ultrasound transducers, in any reservoir geometry.

Acknowledgments

JG and BR acknowledge support from Army Research Office contract# W911NF-14-1-0565 and National Aeronautics and Space Agency award# NNX15AP30H.

References

[1]Grzelczak M, Vermant J, Furst EM, Liz-Marzán LM (2010) Directed Self-Assembly of Nanoparticles. *ACS Nano* **4**(7):3591-3605.

[2]Nie Z, Petukhova A, Kumacheva E (2010) Properties and emerging applications of self-assembled structures made from inorganic nanoparticles. *Nat Nanotechnol* **5**:15-25.

[3]Darling SB (2007) Directing the self-assembly of block copolymers. *Prog Polym Sci* **32**: 1152-1204.

[4]Chen Y, Liu H, Ye T, Kim J Mao C (2007) DNA-directed assembly of single-wall carbon nanotubes. *J Am Chem Soc* **129**:8696-8697.

[5]Hermanson KD, Lumsdon SO, Williams JP, Kaler EW, Velev OD (2001) Dielectrophoretic assembly of electrically functional microwires from nanoparticle suspensions. *Science* **294**:1082-1086.

[6]Promislow JHE, Gast AP (1996) Magnetorheological fluid structure in a pulsed magnetic field. *Langmuir* **12**:4095-4102.

[7]Raeymaekers B, Pantea C, Sinha DN (2011) Manipulation of diamond nanoparticles using bulk acoustic waves. *J Appl Phys* **109**:014317.

[8]Kamat PV, Thomas KG, Barazzouk S, Girishkumar G, Vinodgopal K, Meisel D (2004) Self-assembled linear bundles of single wall carbon nanotubes and their alignment and deposition as a film in a dc field. *J Am Chem Soc* **126**:10757-10762.

[9]Fujiwara M, Oki E, Hamada M, Tanimoto Y, Mukouda I, Shimomura Y (2001) Magnetic orientation and magnetic properties of a single carbon nanotube. *J Phys Chem A* **105**(18):4383-4386.

[10]Bernassau AL, Courtney CRP, Beeley J, Drinkwater BW, Cumming DRS (2013) Interactive manipulation of microparticles in an octagonal sonotweezer. *Appl Phys Lett* **102**:164101.

[11]Evander M, Nilsson J (2012) Acoustofluidics 20: Applications in acoustic trapping. *Lab Chip* **12**:4667-4676.

[12]Yamakoshi Y, Koitabashi Y, Nakajima N, Miwa T (2006) Yeast cell trapping in ultrasonic wave field using ultrasonic contrast agent. *Jpn J Appl Phys* **45**(5B):4712-4717.

[13]Yamakoshi Y, Nakajima N, Miwa T (2007) Microbubble trapping by nonlinear bubble oscillation using pumping wave. *Jpn J Appl Phys* **46**(7B):4847-4850.

[14]Coleman JN, Khan U, Blau WJ, Gun'ko YK (2006) Small but strong: A review of the mechanical properties of carbon nanotube–polymer composites. *Carbon* **44**:1624-1652.

[15]Shalaev VM (2007) Optical negative-index metamaterials. *Nat Phot* **1**:41-48.

[16]Corbitt SJ, Francoeur M, Raeymaekers B (2015) Implementation of optical dielectric metamaterials: A Review. *J Quant Spectrosc Radiat Transfer* **158**:3-16.

[17]Han T, Bai X, Thong JTL, Li B, Qiu CW (2014) Full control and manipulation of heat signatures: cloaking, camoufl age and thermal metamaterials. *Adv Mater* **26**:1731-1734.

[18]Barmatz M, Collas P (1985) Acoustic radiation potential on a sphere in plane, cylindrical, and spherical standing wave fields. *Acoust Soc Am* **77**(3):928-945

[19]Greenhall J, Guevara Vasquez F, Raeymaekers B (2013) Continuous and unconstrained manipulation of micro-particles using phase-control of bulk acoustic waves. *Appl Phys Lett* **103**:074103.

[20]Kozuka T, Yasui K, Tuziuti T, Towata A, Iida Y (2007) Noncontact acoustic manipulation in air. *Jpn J Appl Phys* **46**(7B):4948-4950.

[21]Grinenko A, Ong CK, Courtney CRP, Wilcox PD, Drinkwater BW (2012) Efficient counter-propagating wave acoustic micro-particle manipulation. *Appl Phys Lett* **101**:233501.

[22]Courtney CRP, Drinkwater BW, Demore CEM, Cochran S, Grinenko A, Wilcox PD (2013) Dexterous manipulation of microparticles using Bessel-function acoustic pressure fields. *Appl Phys Lett* **102**:123508.

[23]Courtney CRP, Demore CEM, Wu H, Grinenko A, Wilcox PD, Cochran S, Drinkwater, BW (2014) Independent trapping and manipulation of microparticles using dexterous acoustic tweezers. *Appl Phys Lett* **104**:154103.

[24]Wrobel LC (2002) *The Boundary Element Method, Applications in Thermo-Fluids and Acoustics* (John Wiley & Sons, Hoboken).

[25]Gor'kov LP (1962) On the forces acting on a small particle in an acoustical field in an ideal fluid. *Sov Phys Dokl* **6**(9):773-775.

[26]Parlett BN (1998) *The Symmetric Eigenvalue Problem* (Prentice-Hall, Inc., Upper Saddle River).

[27]Forsyth DA, Ponce J (2012) *Computer Vision, a Modern Approach* (Prentice Hall, Upper Saddle River) p. 131.